Electronic Supporting Information for "Fundamentals of Soft Thermofluidic System Design"

Praveen Kotagama [a] , Kenneth Manning [a] , and Konrad Rykaczewski [a,*]
a. School for Engineering of Matter, Transport and Energy, Arizona State University, Tempe, AZ 85287, USA. Email: konradr@asu.edu

1. The Graetz problem and the thermal boundary layer thickness

Hydrodynamically developed but thermally develping Hagen-Poiseuille flow was treated for the first time by Graetz and is known as the Graetz problem. When not actuated, our setup closely resembles this classic problem (see ref. 1, p.120-128 for description and solutions for both classical wall boundary condition). We use the Leveque solution for a constant heat flux scenario to evaluate the local Nusselt number[2] and estimate the boundary layer thickness in our system:

$$x_* = \frac{x/D}{Re_D Pr}$$

$$Nu_x = 4.364 + 8.68(10^3 x_*)^{-0.506} \exp(-41x_*), x_* \geq 0.001 \quad (1)$$

By substituting variables corresponding to our initial and final tube length, we obtain $x_* = (x/D)/(RePr)$ of 0.033 and 0.044 that according to the above equation corresponds to local Nu_x of 4.75 and 4.58 based (vs. Nu_{dev} of 4.36 in the developed region, illustrated in Fig.S1). Consequently, the flow is thermally developing across the entire length of our stretchable segment. To estimate thickness of the boundary layer at the tube exit, we can use the following scaling relation:

$$\frac{Nu_x}{Nu_{dev}} \sim \frac{k/\delta_{Tx}}{k/r} \sim \frac{r}{\delta_{Tx}} \quad (2)$$

Using this approach, we obtain for both cases $\delta_T \approx 0.9\, r$ at the exit of our tube (r is the radius of the tube).

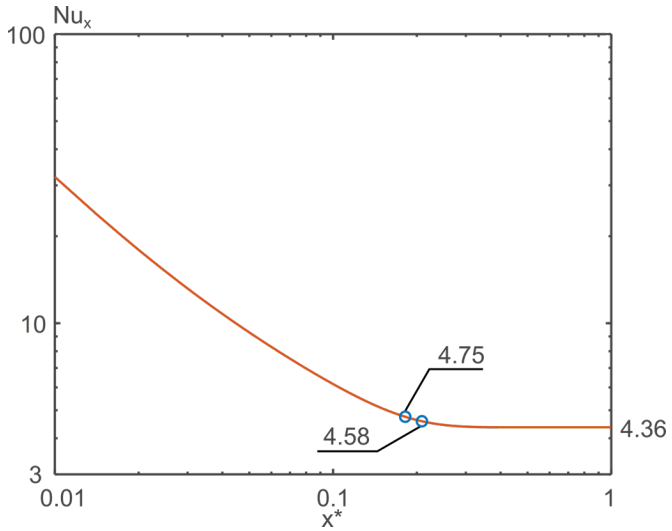

Fig. S1: Local Nusselt number demonstrating developing flow for extended and retracted states.

2. Thermal Performance Variables Considered

In evaluating the behavior of our soft, thermofluidic device we considered multiple characteristic variables. First, we consider the total heat generated by the spring-joule heater and the heat collected by the cooling fluid. The generated heat was calculated with the supply voltage (V) and constant current (I).

$$\dot{Q}_{supply} = VI \tag{3}$$

The electrical resistance of the spring fluctuates with deformation (due to the associated cooling variations) and so there is a slight fluctuation in heat supply, illustrated by the nearly flat line seen in Fig.S2 approximately +/- 1 W. The change in resistance represents a negligible fluctuation in heat generation but is useful in measuring spring temperature as was highlighted in the main text.

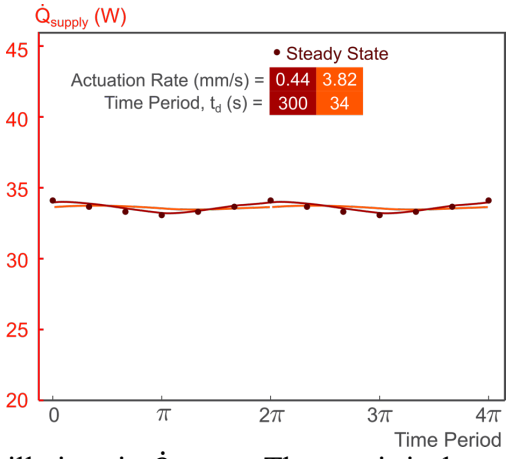

Fig. S2: Plot demonstrating oscillations in $\dot{Q}_{supply}$. The y-axis is the same scale as the plots in Fig. S3 of $\dot{Q}_{water}$ to highlight the negligibility of heat generation fluctuations.

Due to a combination of flow fluctuations and tube deformations, the heat gained ($\dot{Q}_{water}$) by the water also fluctuates. However, it oscillates about $\dot{Q}_{supply}$ indicating effective insulation (see Fig.S3).

$$\dot{Q}_{water} = \dot{m}c_p(T_{out} - T_{in}) \tag{4}$$

In Fig.S3a, we plot the $\dot{Q}_{water}$ as function of the the time period for multiple stretching rates. While impact of the increasing stretching rate on phase and amplitude is observable, these effects are comparable to the total experimental uncertainty. The relatively large uncertainty stems from the compounding effects of uncertainties from several measured variables (temperatures and flow rate).

Equivalent conclusions apply to the impact of actuation rate on the overall heat transfer coefficient (U), the experimental liquid Nusselt (Nu) number, and the total thermal resistance (R_{total}) that we calculated as follows:

$$U = \frac{\dot{Q}_{water}}{A_{inner}(\bar{T}_s - \bar{T}_{fluid})} \tag{5}$$

$$Nu = \frac{h_c D_{inner}}{k_{fluid}} \tag{6}$$

$$R_{total} = \frac{(\bar{T}_s - \bar{T}_{fluid})}{\dot{Q}_{water}} \tag{7}$$

The heat transfer coefficient (h_c) was evaluated using a series thermal resistance model including the tube wall and fluid thermal resistances and the above expression for R_{total}. The total resistance can also be expressed as the sum of these two resistances.

$$R_{total} = R_{conduction} + R_{convection} \tag{8}$$

By substituting the expression for conductive resistance in a cylindrical wall and the conventional definition of convective resistance we obtain the expression below, where all variables except h_c are known.

$$R_{total} = \frac{\ln\left(\frac{D_{outter}}{D_{inner}}\right)}{2\pi k_{wall} L} + \frac{1}{h_c \pi D_{inner} L} \quad (9)$$

Where, $\bar{T}_{fluid} = \frac{T_{in}+T_{out}}{2}$ is the mean fluid temperature, L is the tube length, D_{inner} is the tube inner diameter, $k_{wall} = 0.42\ W/mK$ is the wall thermal conductivity, D_{outter} is the spring inner diameter, A_{inner} is the tube inner wall area, and $k_{fluid} = 0.6\ W/mK$ is the water thermal conductivity.

As in case of the $\dot{Q}_{water}$, in all the calculated variables the impact of tube actuation on phase shift and amplitude change is observable but comparable to the total experimental uncertainty. Conversely, since it was the 'furthest' from the cooling fluid and inner wall undergoing shape change, the spatially avearged spring temperature ($\bar{T}_s$) demonstrated most amplified effects of the tube actuation. Additionally, the $\bar{T}_s$ was measured using the carefully calibrated electrical resistance approach (see below), and thus, had a relatively smaller measurement uncertainty (±1.5°C). Consequently, the relatively small uncertainty combined with the amplified effects of actuation made $\bar{T}_s$ the best choice for our characteristic thermal variable. We note that impacts of actuation on phase shift and amplitude of the other, computed, variables is smaller as compared to changes in $\bar{T}_s$ which is likely due to the "down stream" nature of computed variables and size of our system (i.e. with longer tube length higher amplification would be expected).

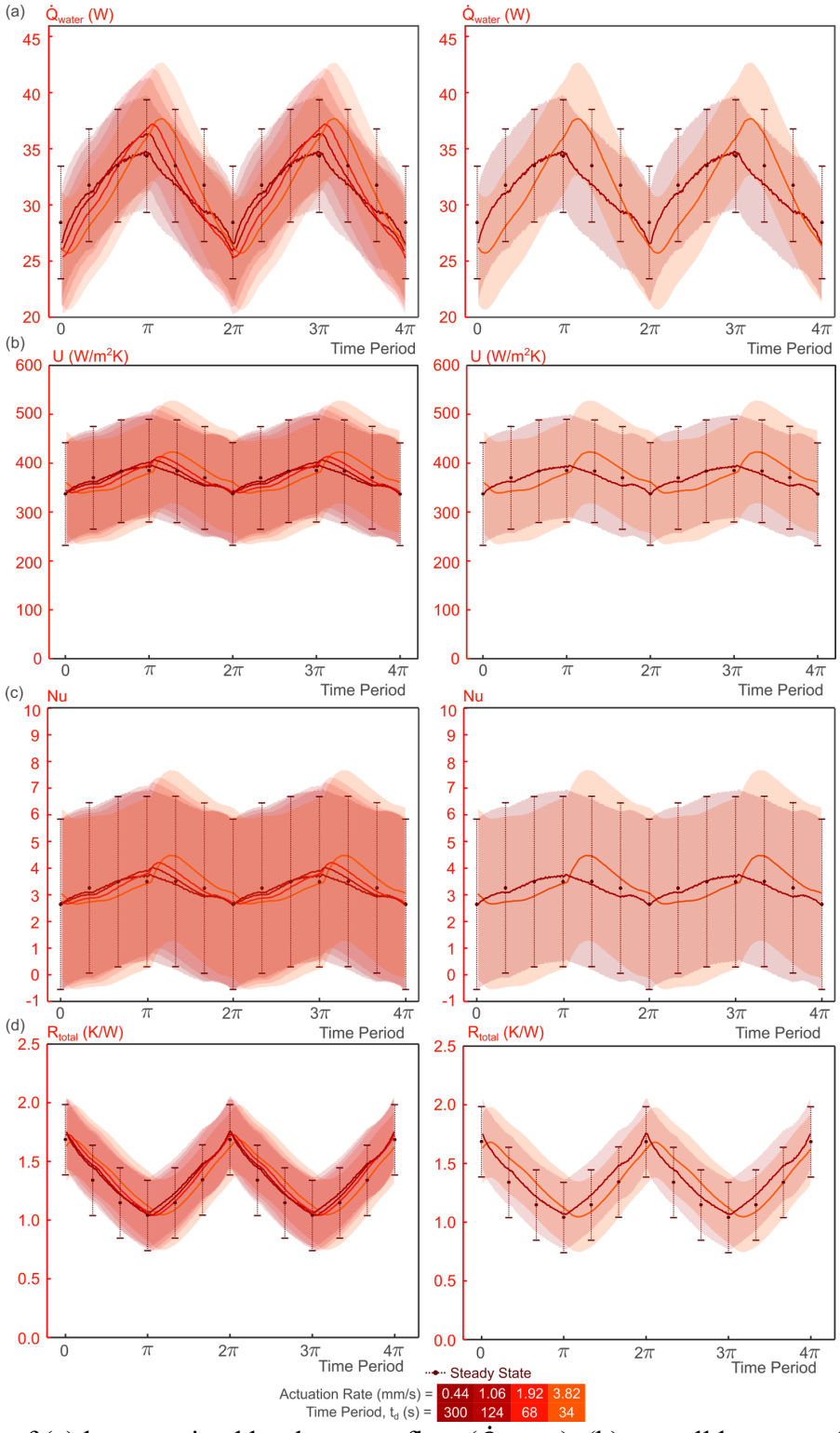

Fig. S3: Plots of (a) heat received by the water flow ($\dot{Q}_{water}$), (b) overall heat transfer coefficient (U) (c) Nusselt number (Nu), and (d) the total thermal resistance (R_{total}) as a function of the time period. In the column on the left all stretching rates are plotted while to facilitate interpretation in the column on the right just the slowest and fastest rates are plotted. The error bars and shaded areas correspond to 95% confidence interval.

3. Liquid metal droplet size-distribution

The liquid metal micro-drop size was measured by image processing a microscope image of a silicone composite (made possible due to the use of a transparent silicone) for over 100 droplets.

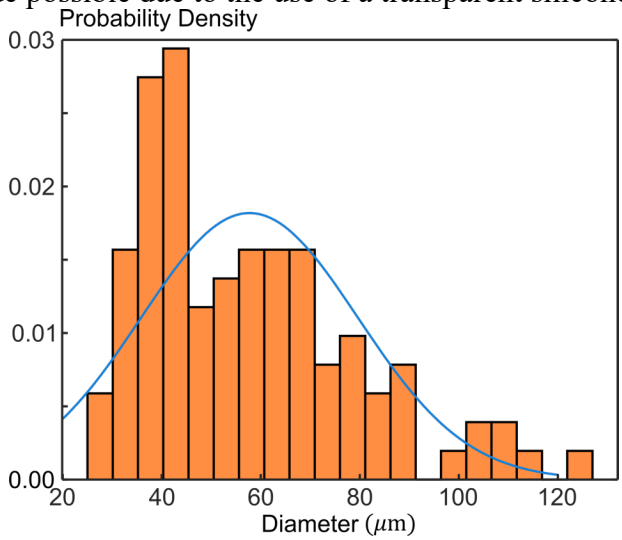

Fig. S4: Plot of measured liquid metal particle size distribution

4. The tube casting process

To make the stretchable heat exchangers, we cast two forms of silicone rubber stoppers to provide compression-based alignment and plugging. The fishing line was centered with the glass tube using rubber stoppers at both ends with an outer diameter (OD rubber stopper) slightly larger than the inner diameter of the glass tube (>5.6 mm) and inner diameter slight smaller than fishing line (<1.9 mm under tension). To align the spring with the fishing line, we cast silicone pieces (ID rubber stopper) with threading and an inner diameter less than 1.9 mm. The spring was threaded into each of these pieces on both sides and pulled along the fishing line from 160 to 275 mm, pre-extending the spring, and since the inner diameter of the stopper was smaller than the fishing line there was enough constriction force on the fishing line to keep the end pieces in place and the spring extended. This configuration was hung vertically and the precured silicone was injected from the bottom at a slow rate of 0.5 ml/min to prevent cavity formation. Once filled, the fishing line was pulled through from the bottom and a weight was hung from it to maintain tension and align the setup vertically. This was allowed to cure at lab temperature for 16 hours and the tubes were removed with the help of IPA as a lubricant.

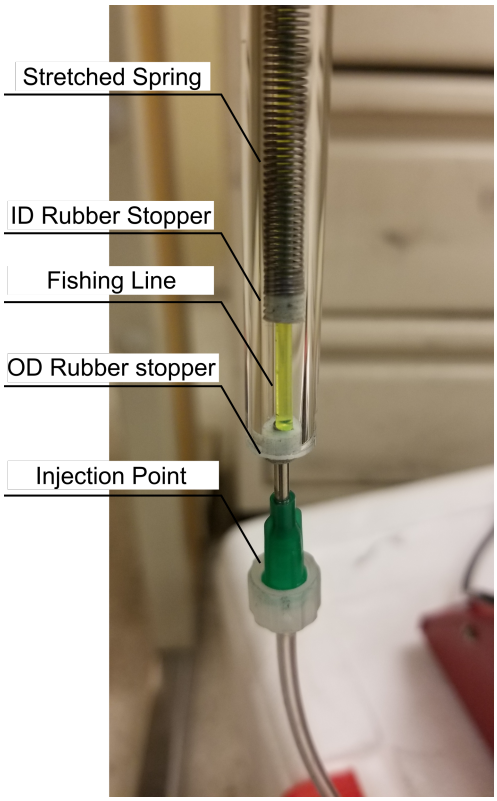

Fig. S5: Picture of the tube casting prior to injection of the silicone composite.

5. The linear actuator calibration

The linear actuator was calibrated to convert the resistance read from the inbuilt potentiometer to the length of stretch, measured relative to the beginning of the stretchable section. Additionally, rates of extension and retraction were measured, and the best fit equation was used to set certain rates on the actuator. The slight deviation from linearity and variations between rates of extension and retraction cause the somewhat arbitrary rates seen in this study. However, we note that we use actual rates calculated from each run for our device time scale calculations.

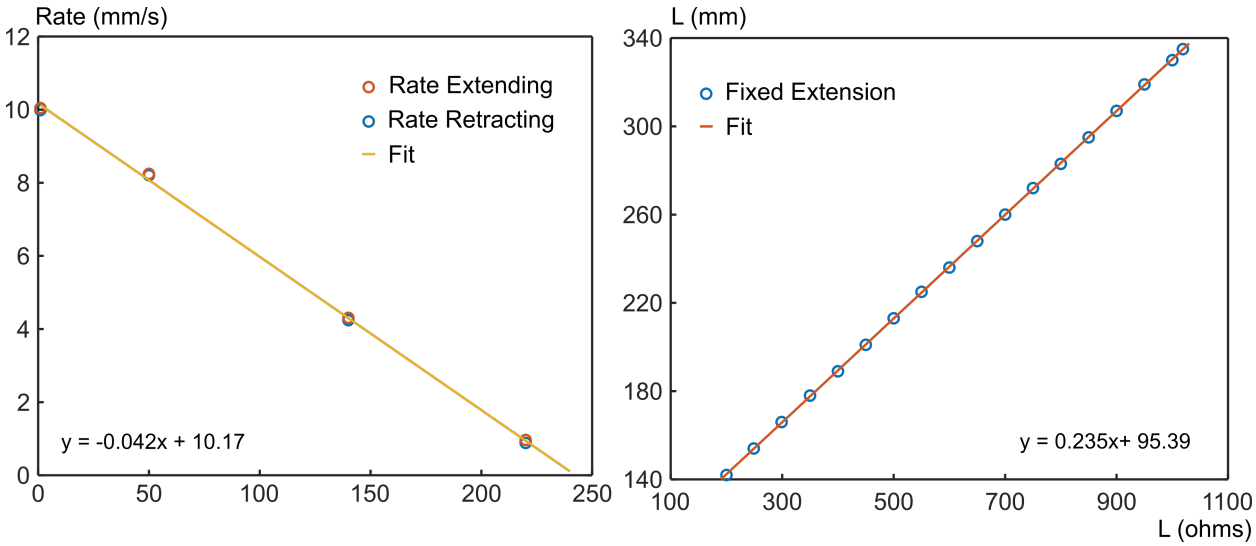

Fig. S6. Plots of the calibration carried out on the linear actuator for the rate of actuation and length stretch vs resistance on the actuators inbuilt potentiometer

6. The mechanical behavior of the tubes

The Poison's effect describes the tube behavior as:

$$D = D_0 \left(\frac{L}{L_0}\right)^{-\nu}$$

We compared our experimental measurements of diameter versus simple simulations for fully constrained and unconstrained tubes made of hyperelastic materials (Comsol Multiphysics 5.2). As clearly seen in Fig. S7, we see an in-between behavior in the shaded region between the two simulations. Additionally, the contraction due to thermal expansion can be seen by comparing the orange lines (2A of heating current) versus the blue lines (no heating).

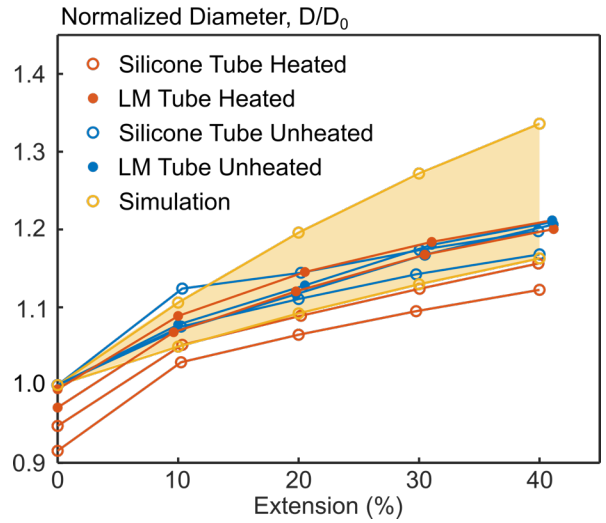

Fig. S7. Plot demonstrating the pseudo constrained behavior of the tube mechanics and the effect of thermal expansion constricting the inner diameter due to thermal expansion

7. The temperature coefficient of the tube-embedded extension spring

The tubes cast with embedded springs were submerged in heated, well mixed, water or silicone oil baths. In this configuration, the baths were allowed to cool down or heat up and the spring resistance versus the bath temperature was transiently measured. This was done for four tubes of which the data was demeaned and compiled to one set of data and used to measure the temperature coefficient. A reference resistance was evaluated at temperatures close to 70°C, for each tested tube.

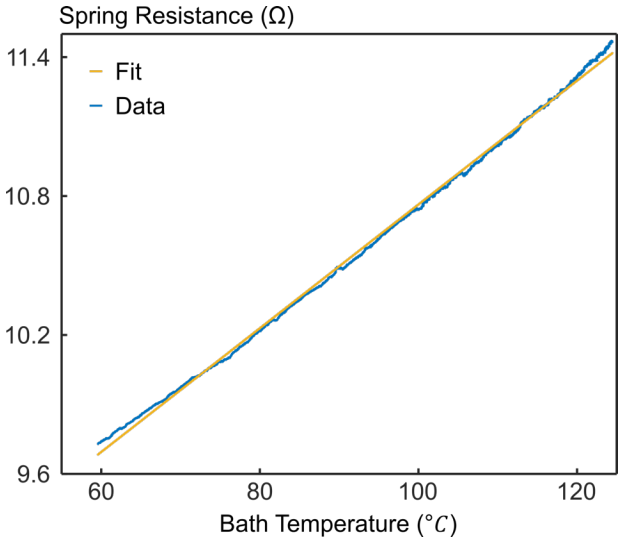

Fig. S8. An example curve of the spring electrical resistance vs bath temperature with a linear fit. One of 4 runs used to evaluate temperature coefficient of resistivity of the embedded spring.

8. Uncertainty Analysis

In Table S1, we list the measured variables and their respective biases that propagate uncertainty in calculations.

Variable	**Bias (b_x)**
Diffusivity (α)	+/- 5 %
Tube Thickness (h)	+/- 0.1 mm
Length (L)	+/- 1 mm
Rate of Actuation (L')	+/- 0.1 mm/s

Table S1: List of biases taken into account and applied in the Taylor series method for the propagation of uncertainty of the time scales.

The Taylor Series Method[2] states that the standard uncertainty is given as a combination of systematic and random standard uncertainties expressed as:

$$u_r^2 = \sum_{i=1}^{J} (\frac{\partial r}{\partial X_i})^2 b_{x_i}^2 + \sum_{i=1}^{J} (\frac{\partial r}{\partial X_i})^2 s_{x_i}^2$$

Where, r represents the variable of interest (t_k/t_d) in our case, X_i represents every variable used in the calculation of r, and, b and s represents the bias and standard deviation of each X_i, respectively. Standard deviations are much lower than the bias in our measurements and so we mainly consider the biases. Thus, after manipulating the equation for t_k/t_d to be a subject of an equation including all the base variables and taking the partial derivatives, the uncertainties were computed. The error bars in the main text represents a 95% confidence interval. The bias of thickness was computed with the same method, where the Taylor series uncertainty was run for the Hagen-Poiseuille law for pressure drop with the biases of each variable listed below.

Variable	**Bias (b_x)**
Viscosity (μ)	+/- 1.24E-5 $Pa.s$
Pressure Drop (ΔP)	+/- 20 Pa
Length (L)	+/- 1 mm
Flow Rate ($\dot{V}$)	+/- 3 ml/min

Table S2: List of biases taken into account and applied in the Taylor series method for the propagation of uncertainty of diameter.

References

[1] Bejan, A. *Convection Heat Transfer*, 4th edition, John Wiley & Sons, Inc., **2013**

[2] Coleman H. W., Steele W. G., *Experimental Uncertainty Analysis for Engineers*, 2nd edition, John Wiley & Sons, Inc., **1999**.